LANGMUIR (ISSN: 0743-7463) 31(5): 1828-1834 (2015)

DOI: 10.1021/la504123k

Growth of nano- and microparticles by controlled reaction-diffusion processes

*Roché M. Walliser[1], Florent Boudoire[2], Eszter Orosz[3], Rita Tóth[2], Artur Braun[2], Edwin C. Constable[1], Zoltán Rácz[4], István Lagzi[3]**

[1]Department of Chemistry, University of Basel, Basel, Switzerland

[2]Laboratory for High Performance Ceramics, Empa, Swiss Federal Laboratories for Materials Science and Technology, Dübendorf, Switzerland

[3]Budapest University of Technology and Economics, P. O. Box H-1521, Budafoki út 8, Budapest, Hungary

[4]MTA-ELTE Theoretical Physics Research Group, Eötvös Loránd University, Budapest, Hungary

AUTHOR EMAIL ADDRESS: lagzi@vuk.chem.elte.hu

RECEIVED DATE (to be automatically inserted after your manuscript is accepted if required according to the journal that you are submitting your paper to)

TITLE RUNNING HEAD

Growth of nano- and microparticles

CORRESPONDING AUTHOR FOOTNOTE *Correspondence to: István Lagzi. Department of Physics, Budapest University of Technology and Economics, H-1111 Budapest, Budafoki út 8, Hungary. E-mail: lagzi@vuk.chem.elte.hu, Tel.:+361-463-1341, Fax:+ 361-463-4180.

Abstract. Synthesis of different size of nano- and microparticles is important in designing nanostructured materials with various properties. Wet synthesis methods lack flexibility to create various sizes of particles (particle libraries) using fixed conditions without the repetition of the steps of the method with a new set of parameters. Here, we report a synthesis method based on nucleation and particle growth in the wake of a moving chemical front in a gel matrix. The process yields well-separated regions (bands) filled with nearly mono-disperse nano- and microparticles, with the size of particles varying from band to band in a predictable way. The origin of the effect is due to an interplay of a precipitation reaction of the reagents and their diffusion that are controlled in space and time by the moving chemical front. The method represents a new approach and a promising tool for fast and competitive synthesis of various sizes of colloidal particles.

KEYWORDS

Nanoparticles; Microparticles; reaction-diffusion; synthesis; gels

1. INTRODUCTION

Synthesis of nano- and microparticles (NPs, MPs) of controlled size and shape has gained importance during the past decades due to the application of such colloidal particles in chemistry, physics, materials sciences and medicine.[1-5] There are two basic challenges in synthesis, the first is to synthesize particles with desired size/shape, and the second is to reduce their polydispersity. The size and the shape of particles typically affect their physical

and chemical properties.[6-15] For example, the catalytic activity of the NPs depends on the particle size[11,12] and the toxicity of gold NPs is known to be size dependent.[6,13,14] The size of sub-micron sized metal oxide particles can determine their photonic properties in water splitting photoelectrodes.[16] Moreover, inherent polydispersity, which arises during the synthesis, can modify the self-assembly resulting in nanostructured materials,[17] thus affecting the overall characteristics of the size-dependent properties of individual NPs and MPs (e.g., their surface plasmon resonance[18] or magnetic susceptibility[19]). There are methods (e.g., synthesis using polymeric stabilizers or reverse micelles), in which a low degree of polydispersity can be achieved.[20-22] Particle synthesis combined with microfluidics provides a method for synthesis of particles with different size and surface compositions (libraries of particles).[23,24] However, in most cases, the particles need to be purified after synthesis.[25] Furthermore, in all those methods using a given set of experimental (e.g., reaction) conditions and parameters provide just a given average size and shape of particles. To obtain mono-disperse particles of various sizes, the experimental conditions and parameters must be changed and the procedure should be repeated.[26] Moreover, for industrial applications, synthesis should be a low cost and rapid process. Design of synthesis methods with fixed conditions and parameters that can provide particles sorted according to their size is rather challenging. Wet synthesis methods are based on redox reactions (e.g., synthesis of noble metal NPs from salt using reducing agents)[27,28] or precipitation reactions (e.g., synthesis of CdS NPs).[29,30] Here we show a novel approach for the synthesis of NPs and MPs using a bottom-up/self-assembly process in which particles with different sizes are spatially sorted into nearly mono-disperse regions. The method is based on using initially separated reagents and controlling the nucleation and growth of particles by a spatio-temporally varied diffusion fluxes.

In order to illustrate our concept, we chose a precipitation process with pattern formation (the classical Liesegang phenomenon) in reaction-diffusion systems.[31] In this emblematic example of self-organization the pattern formation occurs due to the inter-diffusion and chemical reaction between two chemical compounds (the outer and inner electrolytes) resulting in distinct precipitation bands. It has been presented in a previous study that in a Liesegang system (cobalt oxinate) the average size of the formed millimeter sized particles (the size of particles varied between 0.18 mm and 0.28 mm) increases with the band number.[32] As we shall see, these bands play the role of drawers where particles of given size are collected. The experiments are carried out in hydrogels, which prevent both sedimentation of the colloids formed in precipitation reaction and hydrodynamic instabilities that would otherwise destroy the spatial structures. The inner electrolyte is placed in a gel and the outer electrolyte diffuses from a solution or another gel with a high initial concentration. Thus, the pattern formation is driven by a diffusively moving chemical front.

2. EXPERIMENTAL

We used the so-called wet stamping (WETS) method for synthesis of particles (Figure 1a).[33] A solid hydro gel stamp introduces the invading (outer) electrolyte into a thin gelatin film containing a co-precipitating (inner) electrolyte. When the stamp is placed on the film the invading electrolyte diffuses into the gel and precipitate rings are formed around the location where the stamp came into contact with the film. The film thickness is approximately 1 μm. The gelatin film (10 w%, ACROS) containing the inner electrolyte (0.01 M $K_2Cr_2O_7$, ACROS, extra pure 99.5%) and NH_4OH (0.028 M, ACROS) is produced by spin-coating the hot gelatin solution (65°C) on a silicon wafer (700 rpm) and which is than allowed to dry for 24 hours at ambient temperature. The agarose stamp is made of an agarose solution (6 w% - OmniPur Agarose, Merck - prepared with degassed milliQ water) which is heated in a

microwave oven and poured on a pre-shaped polydimethylsiloxane (PDMS) mask containing cylindrical features of 500 μm in diameter with the distance between the features being 1 mm. The degassed and cooled agarose block is removed from the mask, cut into 0.4 cm × 0.4 cm pieces (3 × 3 pins) and soaked in $AgNO_3$ solution (0.3 M, ACROS, extra pure 99.85%). After 2 days the soaked stamps are dried on a filter paper for 2 minutes and placed on the gelatin films for 2 hours. After removing the agarose stamp from the gelatin film, all samples were dried and sputter-coated with gold, and examined with scanning electron microscopy (REM - FEI Nova Nano SEM 230).

3. RESULTS AND DISCUSSUION

As the silver nitrate diffuses out of the stamp, the reaction between silver and dichromate ions results in a reaction product near the pins that transforms into precipitate if the local concentration of the reaction product reaches a threshold concentration (Figure 1a). The precipitation process is fast compared to diffusion and it depletes the inner electrolyte (potassium dichromate) near the zone lowering its local concentration. Therefore, the local concentration of the reacting product remains below the precipitation threshold, and a new separate band forms again only at a distance from the existing band where this threshold is reached again. This process occurs repeatedly creating numerous precipitation rings around the features of the stamp (Figure 1b). The process described above is known as Liesegang pattern formation, or more general, quasi-periodic precipitation.[31,34] We investigated the structure of the Liesegang bands and found that the zones contain particles as observed in earlier experiments,[32] and the average particle size increases with distance from the junction point of the electrolytes (Figure 2a). Interestingly, we found particles in between the bands as well. Their density is much lower and, furthermore, they are much smaller than the particles in the bands, their sizes in the first zones are smaller than 100 nm (Figure 2b).

From the technological point of view it is important to know and understand the dependence of the average size of particles on material parameters. To derive this dependence theoretically, we consider the Liesegang dynamics after the n-th band has formed.[35,36] Liesegang dynamics includes a diffusion front of the outer electrolyte and a reaction between the outer and inner electrolytes according to the reaction A + B → C, where A, B and C denote the outer electrolyte, the inner electrolyte and the reaction product, respectively. This reaction product can further turn into precipitate.[35-37] As shown in Figure 3, the diffusion front $x_f(t) = \sqrt{2D_f t}$ is past the n-th band ($x_f > x_n$ and D_f is the diffusion coefficient of the front, which depends on the diffusion coefficients and on the initial concentration of the electrolytes). The concentration of the reaction product (C) which will turn into the precipitation particles at $x_f(t)$ is maximal and $c_{max}(t)$ increases as the front moves farther away from the band. As $c_{max}(t)$ approaches the spinodal value c_s, the rate of the formation of nucleation centers increases. The nucleation centers deplete the reaction product within a radius of $\sqrt{2D_c \delta t}$, where δt is the time after the nucleation started, so that no new centers form once the depleted regions fill the space. Using the above picture, the size of the particles can be determined as follows. Let the number of centers in a volume V be N_c. Then the average distance l between the centers can be calculated as

$$l = \left(\frac{V}{N_c} \right)^{1/3}, \qquad (1)$$

and if we recall now that a constant concentration of reaction product (C) is left behind the front (c_0)[36], then Eq. 1 gives the radius of the particles r_p through the equality

$$c_0 V = N_c c_p \frac{4\pi}{3} r_p^3, \qquad (2)$$

where c_p is the concentration of the reaction product in the particles which we assume to be a constant and independent of the band number. Thus

$$r_p = \left(\frac{3c_0 V}{4\pi c_p N_c} \right)^{1/3} = l \left(\frac{3c_0}{4\pi c_p} \right)^{1/3} \sim l, \tag{3}$$

and the time-evolution of $l(t)$ determines the time evolution of $r_p(t)$.

An estimate for $l(t)$ is given by

$$l = \sqrt{2D_c \delta t}\,, \tag{4}$$

thus the task is to estimate the time available for the centers of nucleation to collect the reaction product C before the depleted regions start to overlap.

In order to calculate δt, we assume that we are in the asymptotic regime of band formation, i.e. the band number n is large and the front moves slowly and, accordingly, the maximum value of the concentration of the reaction product grows slowly in the front region (Figure 3). We can see this calculating $c_{\max}(t)$ from the condition that the incoming flux, j_{in}, of reagent A is equal to that, j_{out}, of the reaction product C leaving the front region (Figure 3)

$$D_a \frac{a_0}{x_f(t)} = D_f \frac{c_{\max}(t)}{x_f(t) - x_n} \tag{5}$$

yielding

$$c_{\max}(t) = \frac{D_a a_0}{D_c} \left(1 - \frac{x_n}{x_f(t)} \right) = \frac{D_a a_0}{D_c} \left(1 - \frac{x_n}{\sqrt{2D_f t}} \right), \tag{6}$$

where D_a is the diffusion coefficient of the reagent A while a_0 denotes the concentration of A at the gelatin-agarose stamp interface (placed at the origin). We can see now that $c_{\max}(t)$ indeed increases slowly for large times since $\dot{c}_{\max}(t) \sim t^{-3/2}$.

Nucleation mainly occurs in the $c \approx c_{\max}$ region. Let us assume that there is a lower limit $c \approx c_1$ where the nucleation rate is still slow but starts to be appreciable, i.e. the number of nucleation centers formed per unit time is given by

$$R_1 = Q_0 e^{-\beta \delta F(c_1)} V\,, \tag{7}$$

where $F(c_1)$ is the free energy barrier to nucleation at c_1 concentration of particles C, β is the inverse temperature, V is the volume of the system, and Q_0 is some unknown amplitude related to the timescale. We also have an upper value $c \approx c_2$ where the nucleation becomes fast and all the regions which have not been depleted are quickly filled with centers of nucleation (this will happen the latest when reaching the spinodal, $c \approx c_s$).

We shall assume that the nucleation centers formed at the initial stages determine the large particles and the distance between them. They are depleting a region around themselves which has a radius $\sqrt{2D_c \delta t}$ where δt is the time the system evolves from c_1 to c_2. Since this radius gives us $l(t) = \sqrt{2D_c \delta t}$, all we have to do is to calculate δt.

In order to obtain δt, we need to calculate the times t and $t + \delta t$ when the maximum concentrations of the reaction product reach the values c_1 and c_2, i.e. using Eq. 6 we need to solve the following two equations

$$c_1 = \frac{D_a a_0}{D_c}\left(1 - \frac{x_n}{\sqrt{2D_f t}}\right), \tag{8}$$

$$c_2 = \frac{D_a a_0}{D_c}\left(1 - \frac{x_n}{\sqrt{2D_f (t+\delta t)}}\right). \tag{9}$$

Since we are in the asymptotic regime, and we can expand the second equation to obtain

$$c_2 = \frac{D_a a_0}{D_c}\left(1 - \frac{x_n}{\sqrt{2D_f (t+\delta t)}}\right) = c_1 + \frac{D_a a_0}{D_c}\frac{x_n}{\sqrt{2D_f t}}\frac{\delta t}{t}. \tag{10}$$

Using now the above formulae when the (n + 1)th band is forming, i.e. $t \approx t_{n+1}$ and $\sqrt{2D_f t_{n+1}} = x_{n+1}$, we can write

$$c_2 - c_1 = \frac{D_a a_0}{D_c} \frac{x_n}{x_{n+1}} \frac{\delta t}{2t_{n+1}}. \tag{11}$$

Since $x_n / x_{n+1} = 1/(1+p)$ where p is constant, the so-called spacing coefficient[33,36], we can further simplify to have the final expression

$$\delta t = \frac{2(c_2 - c_1) D_c (1+p)}{D_a a_0} t_{n+1}. \tag{12}$$

Substituting the result for δt into the expression for $l(t)$ (Eq. 4), we obtain

$$l = \sqrt{2D_c \delta t} = \sqrt{2D_c \frac{2(c_2 - c_1) D_c (1+p)}{D_a a_0} t_{n+1}} \sim \sqrt{2D_c t_{n+1}} \sim x_n. \tag{13}$$

Thus we have the following result. The distance between the large particles in the n-th band is proportional to x_n. Using now Eq. 3, we find that the radius of a particle as

$$r_p \sim l \sim x_n. \tag{14}$$

We have arrived at the main theoretical result of our work, namely, we found that there is a linear correlation between the size of the particles and position of the band measured from the gelatin-agarose stamp interface.

The nontrivial result of the above calculations is that, due to the general diffusive scaling present in the dynamics of the formation of the Liesegang bands, one finds that the $\delta t \sim t_n$ which can be interpreted as if the particles had the time t_n for growth. This is why one can make contact with experiments on crystal growth where the size of crystals satisfy the well-known time-size relationship $r \sim \sqrt{t}$ similarly to our case (Eq. 14).[38] Figure 4 shows the experimental results for particle diameter in the precipitation bands and in between the bands. The trend is the same for both cases, the size of particles scales linearly with distance of the band measured from the junction of the electrolytes. The size of particles in the interband region is much smaller than in the bands. Our theory does not take into account large fluctuations and the presence of impurities and, consequently, predicts no nucleation events in

the interband regions, and we have no estimates for the size of the particles there. We note that the size of the particles in the interband region near to the agarose pin is lower than 100 nm. Improving the resolution of the bands near the pins may actually uncover even smaller particles.

The agreement between theory and experiment suggests that the nucleation rate at a given position can be obtained from the time evolution of the local concentration of the reaction product (C), c_{max}. Since the dynamics is determined by the front, its velocity is one of the main factors governing the number of nuclei per volume unit that can act as nucleation centers. Those nuclei can grow, and their growth rate and final size are predominantly driven by the rate of formation of the reaction product and its influx from the neighborhood. The above picture also suggests that the nucleation and particle growth can be controlled by the fluxes of the outer electrolyte and the reaction product through the local velocity of the diffusion front. Since the fluxes strongly depend on the position of the reaction front, controlling these fluxes either spatially or temporally can provide flexible control in design of NPs and MPs.

An important issue is the poly-dispersity (the standard deviation of the size) of the particles. This varies with distance and is significantly smaller in the interband region. The latter is less than 10% for the interband particles, which is comparable with the poly-dispersity obtained from other liquid phase synthetic methods.[26] Figure 5 shows in details the probability distribution for the size of particles in the precipitation bands. The basis for the analysis was SEM micrographs shown in Figure 2. As can be seen that average size is shifted towards larger sizes and the distribution is broadened.

We have also studied the average particle size and its standard deviation in a cross section of a band (in the direction of the diffusion flux of the outer electrolyte - silver nitrate) and the results are presented in Figure 6. Similarly, we analyzed particles from Figure 2. The

size distribution is symmetric and the variation is more pronounced for large order bands. In the first band, almost mono-disperse MPs are formed, but they become more poly-disperse with increasing band number. Near the edges of the bands the particles have smaller size compared to particles at the center. This finding is consistent with our earlier discussion. Indeed, near the junction point of the electrolytes, the front moves fast due to the high concentration gradient of the outer electrolyte. This ensures the same nucleation and growth rates in a spatially narrow region thus resulting in the formation of the nearly mono-disperse particles near the stamp interface. Farther from the interface, the degree of homogeneity of the nucleation zone is lessened due to the slower motion of the reaction front and due to the increased width of the front.[39] This leads to inhomogeneities both in the rate of the emergence of the reaction product and in the rate of growth of particles which, in turn, may be the reason for the poly-dispersity observed in the experiments at large band order. To have a more sophisticated picture on the morphology of particles, we used a 3D dual beam scanning electron microscope (SEM-FIB: SEM - FEI Helios Nano Lab 650). These additional investigations verified that particles have spherical shape (Figure 7).

In our method, the diffusion of chemicals plays a crucial role. Thus, from the practical point of view, effectivity and speed of the process may be questioned since mass transport by diffusion is usually considered as a slow process. It is indeed a problem at macroscale since the characteristic diffusion length (diffusion distance – x_{cr}) is related to the characteristic diffusion time (t_{cr}) through $x_{cr} = \sqrt{2Dt_{cr}}$, where D is the diffusion constant of the diffusive species. For macroscale (a few centimeters range), and for small hydrated ions in water (D = 10^{-9} m^2/s) the characteristic diffusion time obtained from the above relation is of the order of a day. However, in our setup, where the characteristic diffusion length (the half distance between the pins) is several hundred μm, the characteristic diffusion time is in order of minutes. Therefore, the time is not a limitation factor.

4. CONCLUSION

We have demonstrated a concept for a competitive, fast and low-cost method for synthesis of NPs and MPs. In this bottom-up approach, the different size of NPs and MPs are self-assembled into spatially well separated domains (bands or regions between the bands) with controllable and predictable particle size. There are several factors that affect the particle size, e.g., temperature, the initial concentrations of reagents, the thickness and the chemical composition of the gel film, thus changing the experimental setup and parameters can provide an easy way of controlling the size ranges of NPs and MPs. This method to engineer various size NPs and MPs in one setup could provide a promising and versatile tool for material science. An obvious next step would be to apply this idea to synthesize NPs and MPs based on redox reaction, [40] where a metal salt and reducing agents could be spatially separated, and the spatio-temporal variation of the local concentration and of the fluxes of the reagents would control the particle size and/or shape.

ACKNOWLEDGMENT

This work was supported by the Hungarian Research Fund (OTKA K104666 and NK100296). Financial support for R.W. and F.B. by the Swiss National Science Foundation under project # SNF 200021-137868, and for R.T. by the Marie Heim-Vögtlin Program under project # PMPDP2-139698 is gratefully acknowledged.

The authors declare no competing financial interest.

REFERENCES

(1) Anker, J. N.; Hall, W. P; Lyandres, O.; Shah, N. C.; Zhao, J.; Van Duyne, R. P. Biosensing with Plasmonic Nanosensors. *Nat. Mater.* **2008**, *7*, 442–453.

(2) Barnes, W. L.; Dereux, A.; Ebbesen, T. W. Surface plasmon subwavelength optics. *Nature* **2003**, *424*, 824–830.

(3) Chon, J. W. M.; Bullen, C.; Zijlstra, P.; Gu, M. Spectral encoding on Gold Nanorods Doped in a Silica Sol–Gel Matrix and Its Application to High ‐ Density Optical Data Storage. *Adv. Funct. Mater.* **2007**, *17*, 875–880.

(4) Peer, D.; Karp, J. M.; Hong, S.; Farokhzad, O. C.; Margalit, R.; Langer, R. Nanocarriers as an Emerging Platform for Cancer Therapy. *Nat. Nanotechnol.* **2007**, *2*, 751–760.

(5) Wang, A. Z.; Langer, R.; Farokhzad, O. C. Nanoparticle Delivery of Cancer Drugs. *Annu. Rev. Med.* **2012**, *63*, 185–198.

(6) Jiang, W.; Kim, B. Y. S.; Rutka, J. T.; Chan, W. C. W. Nanoparticle-Mediated Cellular Response is Size-Dependent. *Nat. Nanotechnol.* **2008**, *3*, 145–150.

(7) Park, T. J.; Papaefthymiou, G. C.; Viescas, A. J.; Moodenbaugh, A. R.; Wong, S. S. Size-Dependent Magnetic Properties of Single-Crystalline Multiferroic BiFeO3 Nanoparticles. *Nano Lett.* **2007**, *7*, 766–772.

(8) Nanda, J.; Narayan, K.S.; Kuruvilla, B. A.; Murthy, G. L.; Sarma, D. D. Sizable Photocurrent and Emission from Solid State Devices Based on CdS Nanoparticles. *Appl. Phys. Lett.* **1998**, *72*, 1335–1337.

(9) Park, S. W.; Jang, J. T.; Cheon, J.; Lee, H. H.; Lee, D. R.; Lee, Y. *J. Phys. Chem. C* Shape-Dependent Compressibility of TiO2 Anatase Nanoparticles. **2008**, *112*, 9627–9631.

(10) Zheng, C.; Du, Y. H.; Feng, M.; Zhan, H. B. Shape Dependence of Nonlinear Optical Behaviors of Nanostructured Silver and Their Silica Gel Glass Composites. *Appl. Phys. Lett.* **2008**, *93*, 143108.

(11) Narayanan, R.; El-Sayed, M. A. Shape-Dependent Catalytic Activity of Platinum Nanoparticles in Colloidal Solution. *Nano Lett.* **2004**, *4*, 1343–1348.

(12) Wei, Y. H.; Han, S. B.; Kim, J.; Soh, S.; Grzybowski, B. A. Photoswitchable Catalysis Mediated by Dynamic Aggregation of Nanoparticles. *J. Am. Chem. Soc.* **2010**, *132*, 11018–11020.

(13) Pan, Y.; Neuss, S.; Leifert, A.; Fischler, M.; Wen, F.; Simon, U.; Schmid, G.; Brandau, W.; Jahnen-Dechent, W. Size-Dependent Cytotoxicity of Gold Nanoparticles. *Small* **2007**, *3*, 1941–1949.

(14) Euliss, L. E.; DuPont, J. A.; Gratton, S.; DeSimone, J. Imparting Size, Shape, and Composition Control of Materials for Nanomedicine. *Chem. Soc. Rev.* **2006**, *35*, 1095–1104.

(15) Xia, Y.; Xiong, Y.; Lim, B.; Skrabalak, S. E. Shape-Controlled Synthesis of Metal Nanocrystals: Simple Chemistry Meets Complex Physics? *Angew. Chem. Int. Ed.* **2009**, *48*, 60–103.

(16) Boudoire, F. ; Tóth, R.; Heier, J. ; Braun, A. ; Constable, E. C. Photonic Light Trapping in Self-Organized All-Oxide microspheroids Impacts Photoelectrochemical Water Splitting. *Energy & Environ. Sci.* **2014**, *7*, 2680–2688.

(17) Kowalczyk, B.; Kalsin, A. M.; Orlik, R.; Bishop, K. J. M.; Patashinski, A. Z.; Mitus, A.; Grzybowski, B. A. Size Selection During Crystallization of Oppositely Charged Nanoparticles. *Chem. Eur. J.* **2009**, *15*, 2032–2035.

(18) Yu, K.; Kelly, K. L.; Sakai, N.; Tatsuma, T. Morphologies and Surface Plasmon Resonance Properties of Monodisperse Bumpy Gold Nanoparticles. *Langmuir* **2008**, *24*, 5849–5854.

(19) Vestal, C. R.; Zhang, Z. J. Synthesis of CoCrFeO4 Nanoparticles Using Microemulsion Methods and Size-Dependent Studies of Their Magnetic Properties*Chem. Mater.* **2002**, *14*, 3817–3822.

(20) Wang, Z. X.; Tan, B. E.; Hussain, I.; Schaeffer, N.; Wyatt, M. F.; Brust, M.; Cooper, A. I. Design of Polymeric Stabilizers for Size-Controlled Synthesis of Monodisperse Gold Nanoparticles in Water. *Langmuir* **2007**, *23*, 885–895.

(21) Hussain, I.; Graham, S.; Wang, Z. X.; Tan, B.; Sherrington, D. C.; Rannard, S. P.; Cooper, A. I.; Brust, M. Size-Controlled Synthesis of Near-Monodisperse Gold Nanoparticles in the 1-4 nm Range Using Polymeric Stabilizers. *J. Am. Chem. Soc.* **2005**, *127*, 16398–16399.

(22) Taleb, A.; Petit, C.; Pileni, M. P.; Synthesis of Highly Monodisperse Silver Nanoparticles from AOT Reverse Micelles: A Way to 2D and 3D Self-Organization. *Chem. Mater.* **1997**, *9*, 950–959.

(23) Valencia, P. M.; Farokhzad, O. C.; Karnik, R.; Langer, R. Microfluidic Technologies for Accelerating the Clinical Translation of Nanoparticles. *Nat. Nanotechnol.* **2012**, *7*, 623–629.

(24) Abou-Hassan, A.; Sandre, O.; Cabuil, V. Microfluidics in Inorganic Chemistry. *Angew. Chem. Int. Ed.* **2010**, *49*, 6268–6268.

(25) Kowalczyk, B.; Lagzi, I.; Grzybowski, B A. Nanoseparations: Strategies for Size and/or Shape-Selective Purification of Nanoparticles. *Curr. Opin. Colloid. In.* **2011**, *16*, 135–148.

(26) Bastus, N. G.; Comenge, J.; Puntes, V. Kinetically Controlled Seeded Growth Synthesis of Citrate-Stabilized Gold Nanoparticles of up to 200 nm: Size Focusing Versus Ostwald Ripening. *Langmuir* **2011**, *27*, 11098–11105.

(27) Pillai, Z. S.; Kamat, P. V. What Factors Control the Size and Shape of Silver Nanoparticles in the Citrate Ion Reduction Method? *J. Phys. Chem. B* **2004**, *108*, 945–951.

(28) Polte, J.; Ahner, T. T.; Delissen, F.; Sokolov, S.; Emmerling, F.; Thünemann, A. F.; Kraehnert, R. Mechanism of Gold Nanoparticle Formation in the Classical Citrate Synthesis Method Derived from Coupled in Situ XANES and SAXS Evaluation. *J. Am. Chem. Soc*. **2010**, *132*, 1296–1301.

(29) Qi, L.; Colfen, H.; Antonietti, M. Synthesis and Characterization of CdS Nanoparticles Stabilized by Double-Hydrophilic Block Copolymers. *Nano Lett.* **2001**, *1*, 61–65.

(30) Al-Ghoul, M.; Ghaddar, T.; Moukalled, T. Pulse-Front Propagation and Interaction During the Growth of CdS Nanoparticles in a Gel. *J. Phys. Chem. B* **2009**, *113*, 11594–11603.

(31) Liesegang, R. E. Über Einige Eigenschaften von Gallerten. *Naturwiss. Wochenschr.* **1896**, *11*, 353–362.

(32) Mandalian, L.; Fahs, M.; Al-Ghoul, M.; Sultan, R. Morphology, Particle Size Distribution, and Composition in One- and Two-Salt Metal Oxinate Liesegang Patterns. *J. Phys. Chem. B* **2004**, *108*, 1507–1514.

(33) Campbell, C. J.; Smoukov, S. K.; Bishop, K. J. M.; Grzybowski, B. A. Reactive Surface Micropatterning by Wet Stamping. *Langmuir* **2005**, *21*, 2637–2640.

(34) Müller, S. C.; Ross, J. Spatial Structure Formation in Precipitation Reactions. *J. Phys. Chem. A* **2003**, *107*, 7997–8008.

(35) Antal, T.; Droz, M.; Magnin, J. ; Rácz, Z. Formation of Liesengang Patterns: A Spinodal Decomposition Scenario. *Phys. Rev. Lett.* **1999**, *83*, 2880–2883.

(36) Rácz, Z. Formation of Liesegang Patterns. *Physica A* **1999**, *274*, 50–59.

(37) Antal, T.; Droz, M.; Magnin, J.; Pekalski, A.; Rácz, Z. Formation of Liesegang Patterns: Simulations Using a Kinetic Ising Model. *J. Chem. Phys.* **2001**, *114*, 3770–3775.

(38) Henisch, H. K.; Hanoka, J. I.; Dennis, J. Growth Rate and Defect Structure of Gel-Grown Crystals. *J. Electrochem. Soc.* **1965**, *112*, 627–629.

(39) Gálfi, L.; Rácz, Z. Properties of the Reaction Front in an A+B-->C Type Reaction-Diffusion Process. *Phys. Rev. A* **1988**, *38*, 3151(R).

(40) Nabika, H.; Sato, M.; Unoura, K. Liesegang Patterns Engineered by a Chemical Reaction Assisted by Complex Formation. *Langmuir* **2014**, *30*, 5047–5051.

FIGURE CAPTIONS

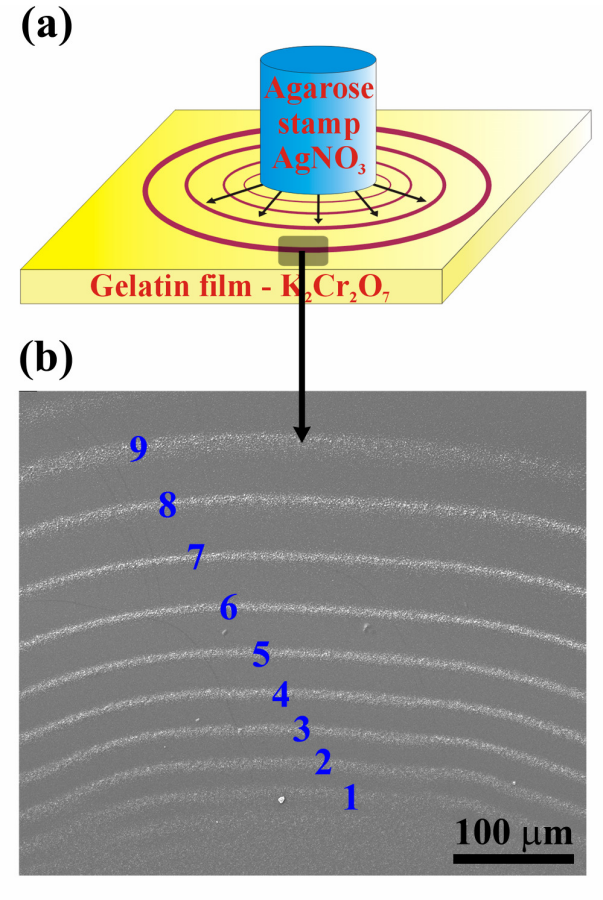

Figure 1. Sketch of the experimental setup using the wet stamping method (a). SEM micrograph of the spatial pattern consisting of quasi-periodic precipitation bands/rings (b). First the band 1 emerged in the wake of the reaction front followed by the consecutive formation of bands No. 2-9.

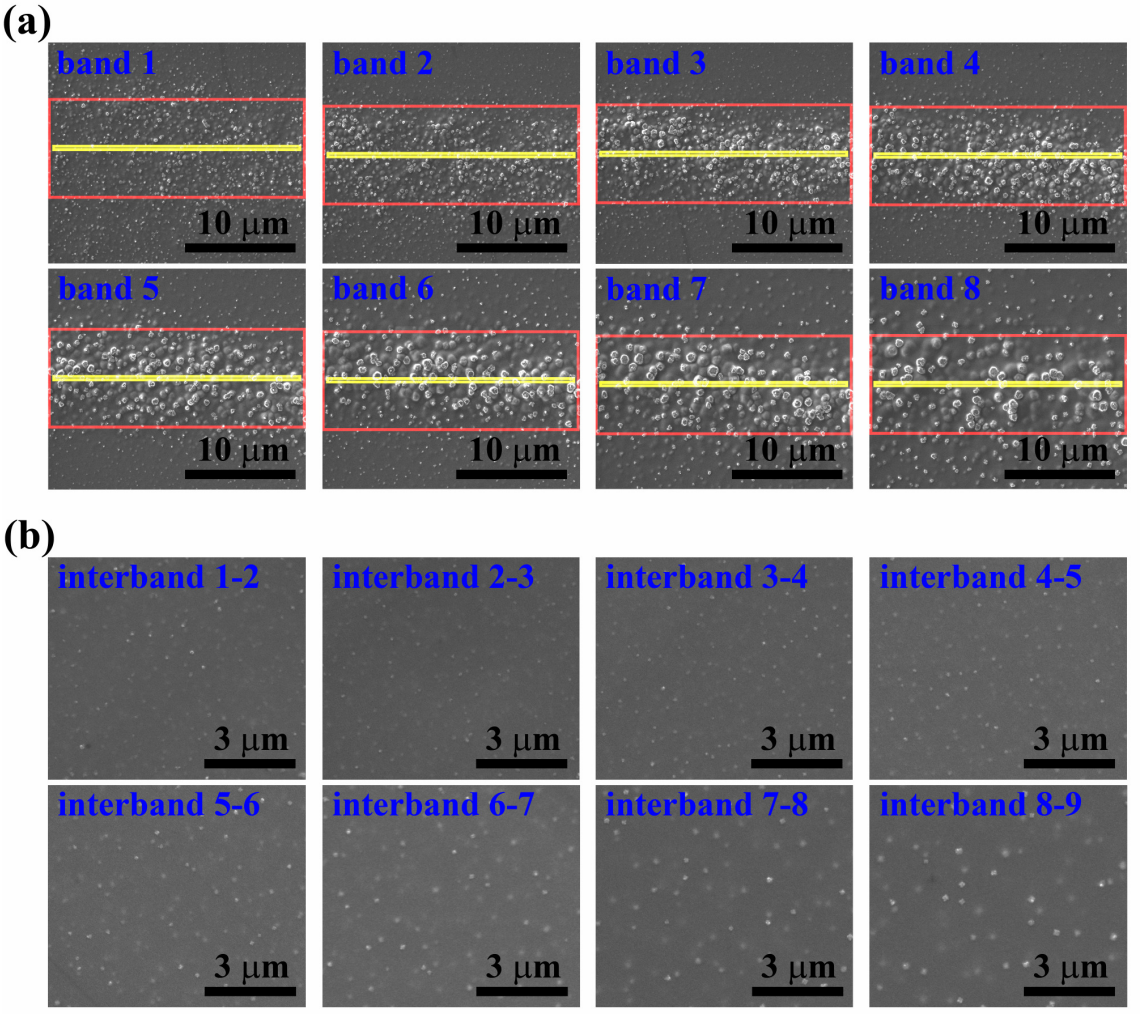

Figure 2. Fine-structure of the bands (a) and the interband regions (b) presented in Figure 1b. Bands and interband region contains nano- and microparticles, whose size varies with the position of the bands.

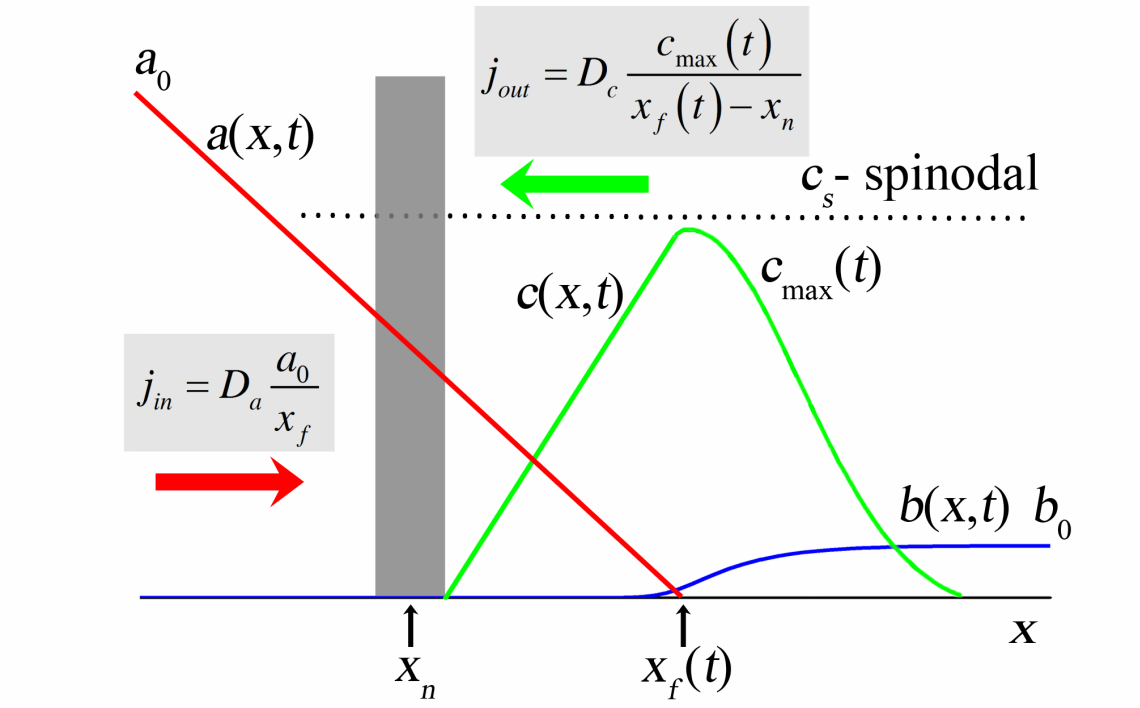

Figure 3. Profile of the concentration of the reaction product, C, ($c(x,t)$ – green line) near the front position $x_f(t) > x_n$ once the n-th band has been formed and the (n + 1)th band is about to form. The concentration of the reagents, $a(x,t)$ and $b(x,t)$, are shown by red and blue, respectively, with their asymptotic value given by a_0 and b_0. The spinodal concentration c_s for the reaction product are shown by dotted line. The incoming flux of the reagents to the front and the outgoing flux of the reaction product are calculated by assuming linear concentration profiles in the vicinity of the reaction zone.

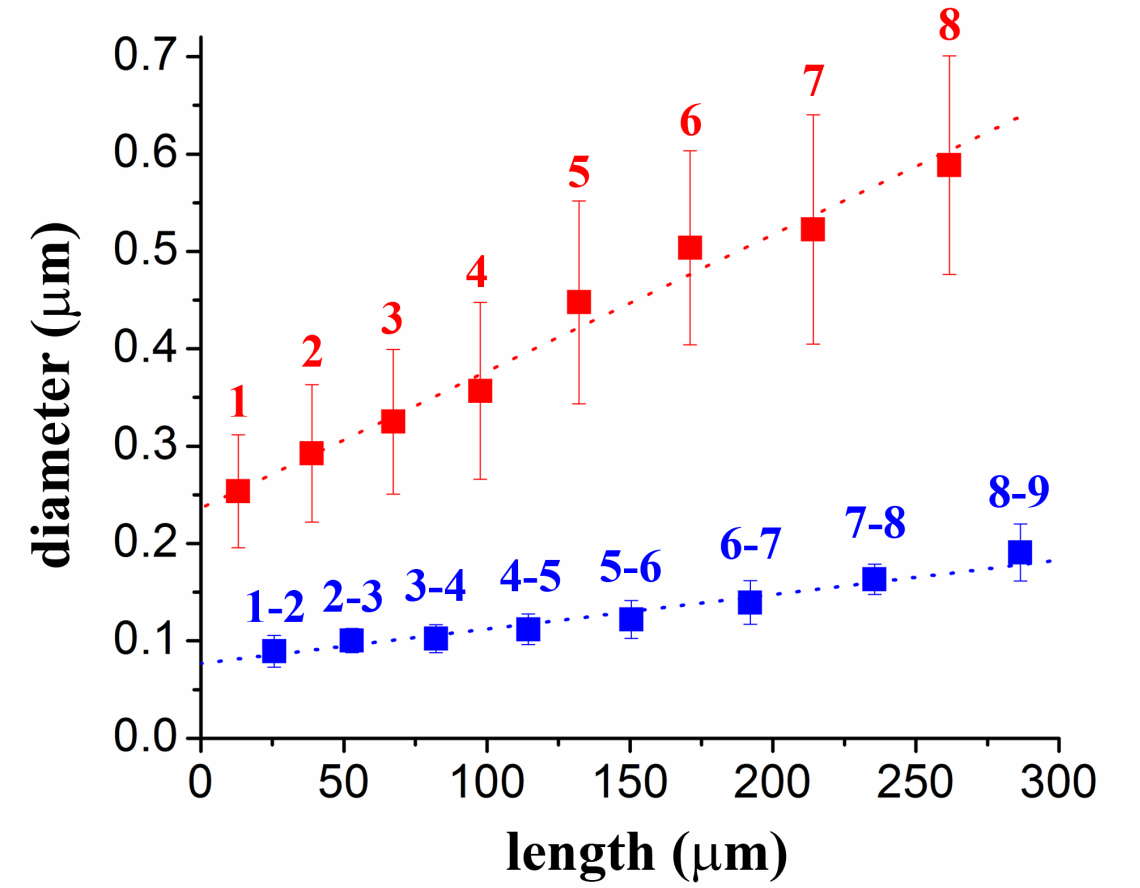

Figure 4. Variation of the diameter of particles in the bands (red symbols, bands were defined as indicated by red boxes in Figure 2) and between the bands (blue symbols) as a function of their distances from the junction point of the electrolytes. The size of the particles was determined using digital image analysis (ImageJ) software. The band numbers are as indicated in Figure 1.

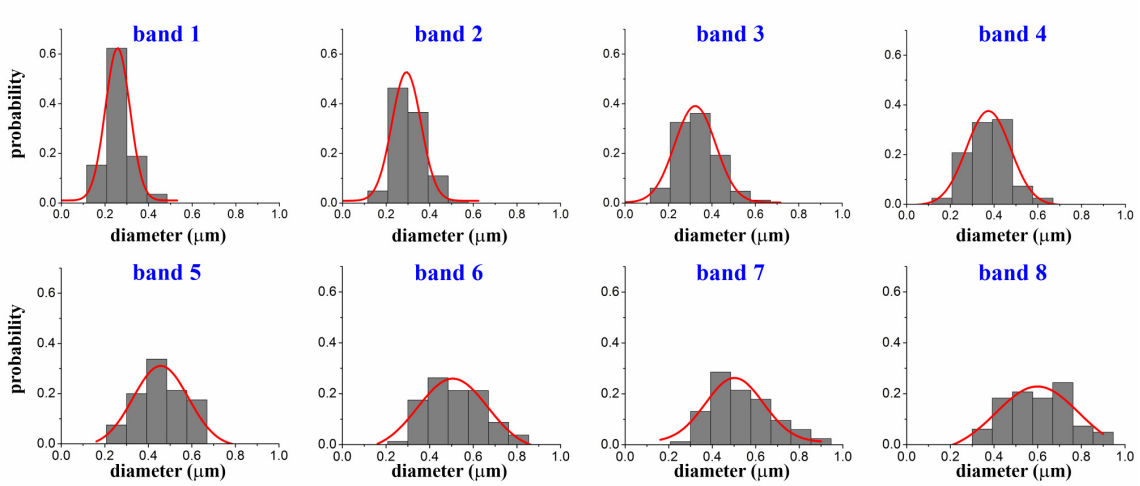

Figure 5. Particle size distributions in the bands. Bands are defined as indicated by red boxes in Figure 2a. Red lines correspond to the fitted Gaussian curves.

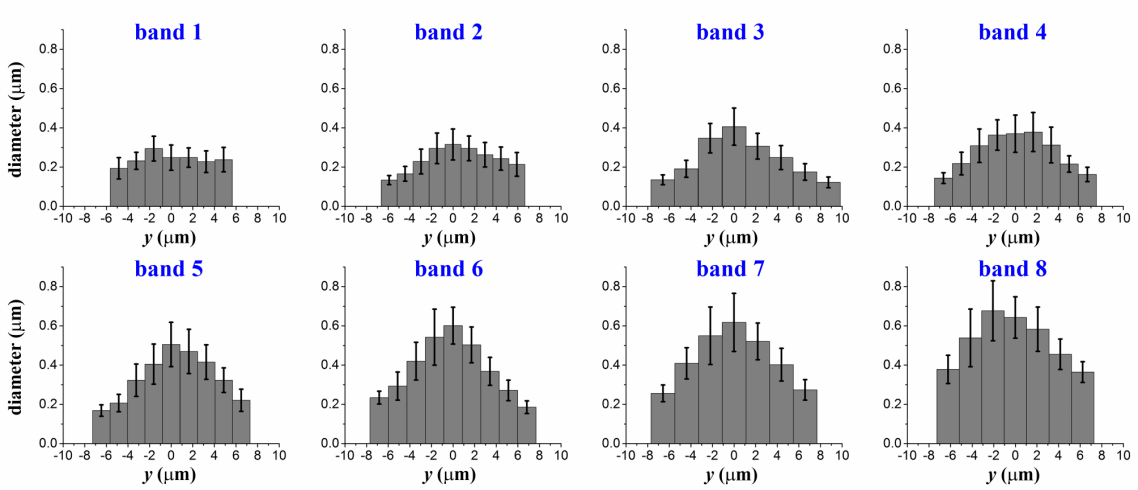

Figure 6. Size of particles in the cross sections of bands (in the direction of the diffusion flux of the outer electrolyte). The distance (y) is measured from the centerline of the bands (yellow line in Figure 2a).

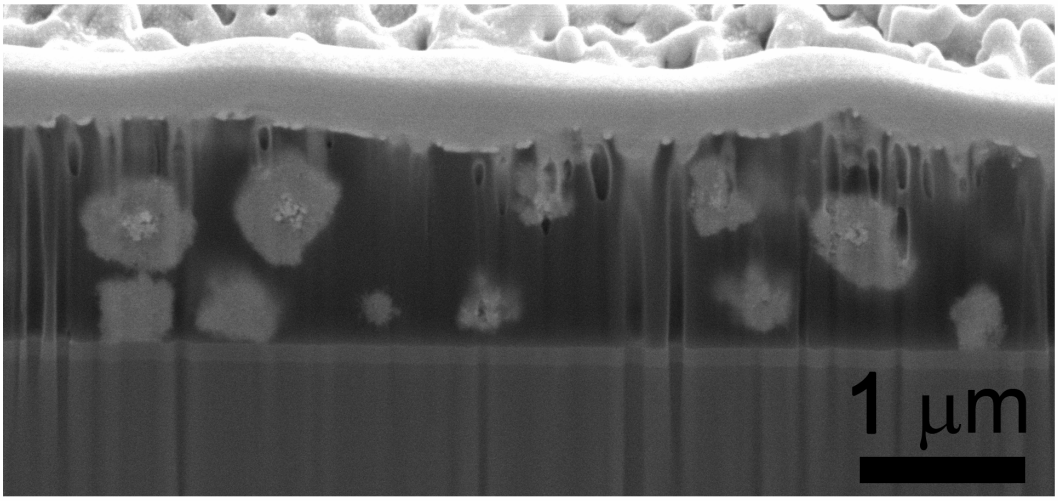

Figure 7. Cross section of a precipitation band using a 3D dual beam scanning electron microscope (SEM-FIB: SEM - FEI Helios Nano Lab 650).

For Table of Contents Use Only

MS title: Synthesis of nano- and microparticles by controlled reaction-diffusion processes

Authors: Roché M. Walliser, Florent Boudoire, Eszter Orosz, Rita Tóth, Artur Braun, Edwin C. Constable, Zoltán Rácz, István Lagzi

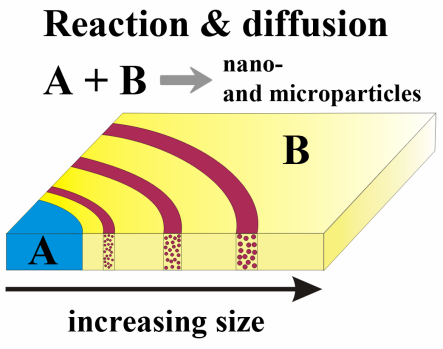

TOC figure